# Supplementary Information for

## Unraveling the dynamics of multiple excited states in a single-molecule transistor

Hao Zhang (张浩)1†, Lijue Chen (陈李珏)1†, Ziheng Yuan (苑子恒)1†, Jingyu Yang (杨靖宇)2,3†, Yu Zhou (周彧)1†, Yixuan Gao (高艺璇)2,3, Zhixin Qiu (邱智鑫)1, Wei Xu (徐伟)1, Zhexiong Zheng (郑哲雄)1, Cankun Zhang (张灿坤)1, Haojie Liu (刘豪杰)1, Kai-Qiang Lin (林楷强)1, Ye Yang (杨晔)1, Jing Li (李晶)1, Junyang Liu (刘俊扬)1*, Shixuan Du (杜世萱)2,3*, Wenjing Hong (洪文晶)1*

[1]State Key Laboratory of Physical Chemistry of Solid Surfaces & IKKEM, College of Chemistry and Chemical Engineering, Xiamen University, Xiamen 361005, China

[2]Beijing National Laboratory for Condensed Matter Physics, Institute of Physics, Chinese Academy of Sciences, Beijing 100190, China

[3]University of Chinese Academy of Sciences, Chinese Academy of Sciences, Beijing 100049, China

†These authors contributed equally: Hao Zhang, Lijue Chen, Ziheng Yuan, Jingyu Yang, Yu Zhou

*Corresponding authors

E-mail: whong@xmu.edu.cn (W. Hong); sxdu@iphy.ac.cn (S. Du); jyliu@xmu.edu.cn (J. Liu)

# Table of Contents

**Supplementary Note 1. Molecular Synthesis**

All reagents were purchased from TCI and used without further purification. The NMR spectra were recorded on a BRUKER AVANCE NEO 500 instrument and Tetramethylsilane (TMS) was used as an internal standard.

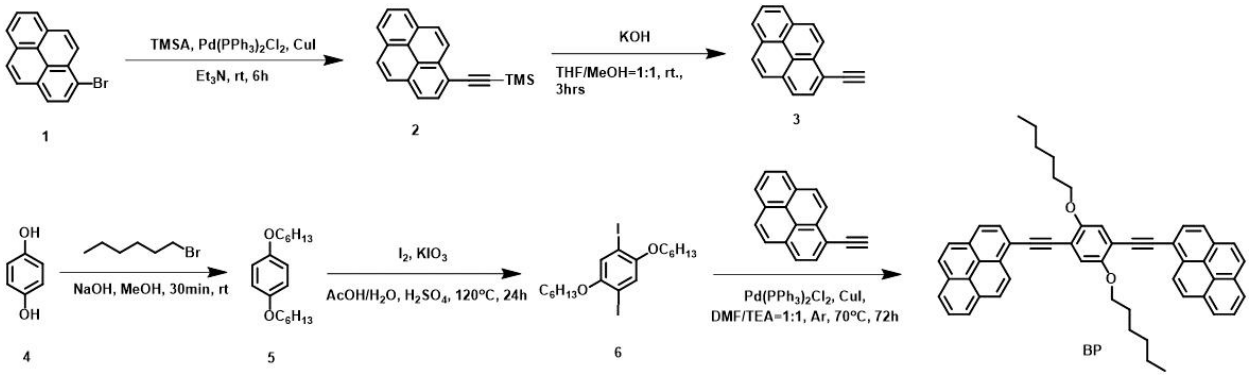


**Supplementary Fig.1 Schematic representations of 1,4-bis(hexyloxy)-2,5-bis(ethynylpyrene)benzene (BP) molecule synthesis**

Synthesis of trimethyl(pyren-1-ylethynyl)silane (**Compound 2**): A mixture of 1-bromopyrene (562 mg, 2 mmol), $Pd(PPh_3)_2Cl_2$ (70 mg, 0.1 mmol), and CuI (4 mg, 0.02 mmol) was dissolved in $Et_3N$ (10 mL). The solution was then degassed and refilled with $N_2$. TMSA (236 mg, 2.4 mmol in 10 mL $Et_3N$) was slowly added to the mixture. The reaction was allowed to proceed at room temperature for 6 hours. The resulting residue was purified using a silica chromatography column (EA/Hex = 1:4) to obtain a yellow solid, which was directly used in the subsequent step without any further purification.

Synthesis of 1-ethynylpyrene (**Compound 3**) [1]: A mixture of trimethyl(pyren-1-ylethynyl)silane (597 mg, 2 mmol), KOH (561 mg, 10 mmol), MeOH (10 mL), and THF (10 mL) was stirred at room temperature for 3 hours. Subsequently, the reaction mixture was extracted with ethyl acetate and washed with brine. After the solvent was evaporated, 1-ethynylpyrene was obtained as a yellow-brown solid. The compound was further purified using a silica chromatography column (DCM/Hex, v/v = 1:20 to 1:10), resulting in the isolation of the product (355 mg, 80% yield). 1HNMR (500 MHz, $CDCl_3$): δ =8.59 (d, 2H, J = 9.1 Hz), 8.17-8.25 (m, 4H), 8.11 (d, 2H, J = 8.5 Hz), 8.0-8.06 (m, 2H), 3.63 (s, 1H) ppm.

Synthesis of 1,4-bis(hexyloxy)benzene (**Compound 5**): To 100 mL of distilled dimethylformamide, hydroquinone (13.21 g, 120 mmol) and potassium hydroxide (27 g, 480 mmol) were added with vigorous stirring for 30 minutes under a nitrogen atmosphere. Subsequently, n-hexyl bromide (59 g, 260 mmol) was added dropwise to the mixture. The reaction was allowed to proceed for 7 hours, after which the mixture was poured into an ample amount of distilled water, resulting in the formation of a light-yellow solid at the upper layer. The crude product was recrystallized with isopropyl and then filtered. The filtered product was washed successively with distilled water and 10% sodium hydroxide, followed by drying under vacuum, yielding a white sheet-like product. This product was directly used in the subsequent step without further purification.

Synthesis of 1,4-bis(hexyloxy)-2,5-diiodobenzene (**Compound 6**)[2]: To a solution of 1,4-Bis(hexyloxy)benzene (1.8 g, 6.5 mmol) in 8 mL of acetic acid, 1 mL of water, and 0.5 mL of $H_2SO_4$, $KIO_3$ (1.08 g, 5.05 mmol) and $I_2$ (1.21 g; 4.77 mmol) were added. The reaction mixture was stirred at 120°C for 24 hours and then cooled to room temperature. Excess iodine was

eliminated by the addition of sodium thiosulfate until the brown color of iodine disappeared. Excess $H_2SO_4$ was neutralized by the addition of $Na_2CO_3$ until the vigorous effervescence ceased. The resulting mixture was extracted with chloroform, dried over $Na_2SO_4$, concentrated, and subsequently purified by column chromatography using silica with hexane as the eluent, yielding the compound as a white crystalline solid (yield = 41%). $^1$HNMR (500 MHz, CDCl3): δ =7.17 (s, 2H), 3.92 (t, 4H, J = 6.45 Hz), 1.79 (m, 4H), 1.3-1.55 (m, 12H), 0.91 (t, 6H, J = 7.05 Hz) ppm.

Synthesis of 1,4-bis(hexyloxy)-2,5-bis(ethynylpyrene)benzene (**BP** molecule) [3]: 1-Ethynylpyrene (61 mg, 0.27 mmol) and 1,4-bis(hexyloxy)-2,5-diiodobenzene (159 mg, 0.3 mmol) were dissolved in a mixture of dry dimethylformamide (10 mL) and triethylamine (10 mL) under a nitrogen atmosphere. To the solution, $[PdCl_2(PPh_3)_2]$ (4.2 mg, 0.006 mmol) and CuI (1.1 mg, 0.006 mmol) were added. After stirring the reaction solution at 70 °C for 36 hours, the solvent was removed under vacuum, resulting in a light-yellow solid. The solid was then purified by silica gel column chromatography (eluent: DCM/hexane; v/v = 1/7). The solvent was evaporated, and the resulting solid was dried under vacuum, yielding a yellow powder. The yellow powder was precipitated with DCM/Hex and subsequently recrystallized with DCM/Hex at a ratio of 1:5 to obtain a single crystal (180 mg, 60% yield). $^1$HNMR (500 MHz, CDCl3): δ =8.89 (d, 2H, J = 9 Hz), 8.03-8.25 (m, 18H), 4.24 (t, 4H, J = 6.4 Hz), 1.69 (m, 4H), 1.69 (m, 4H), 1.36-1.51 (m, 8H), 0.90 (t, 6H, J = 7.15 Hz) ppm. HR-MS: $[M+Na]^+$ calcd for $C_{54}H_{46}O_2Na^+$: 749.3396, found 749.3353.

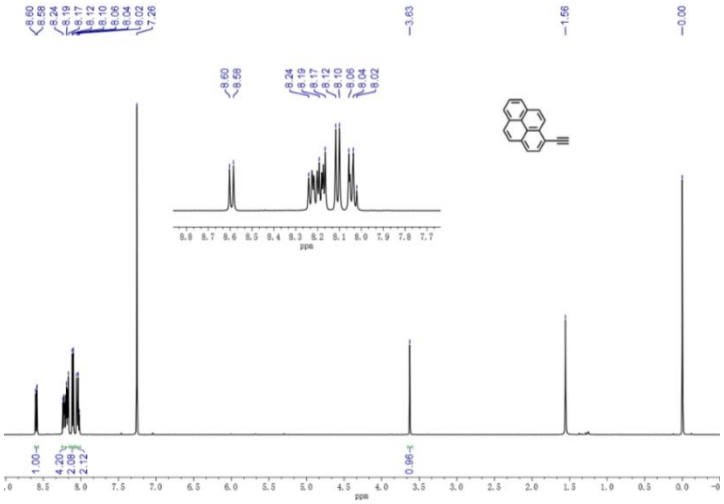

**Supplementary Fig. 2 $^1$HNMR spectrum of 1-ethynylpyrene (Compound 3) in chloroform-D**

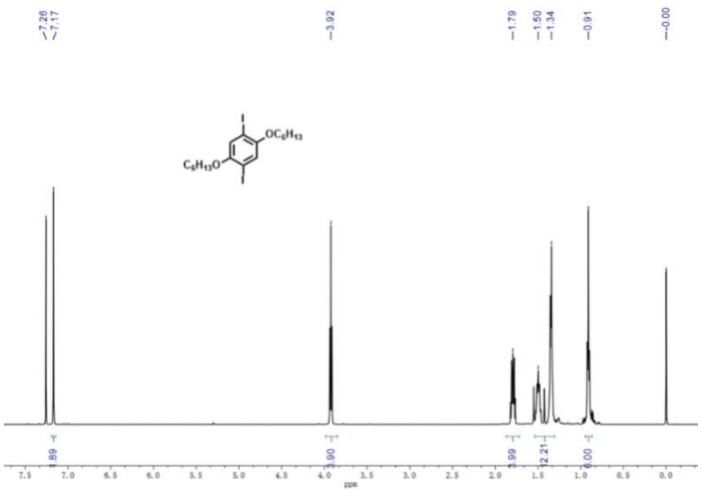

**Supplementary Fig. 3 [1]HNMR spectrum of 1,4-bis(hexyloxy)-2,5-diiodobenzene (Compound 6) in chloroform-D**

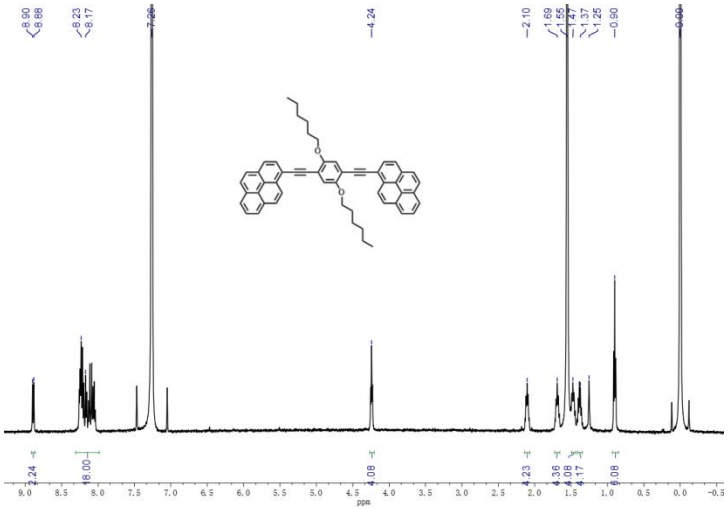

**Supplementary Fig. 4 [1]HNMR spectrum of 1,4-bis(hexyloxy)-2,5-bis(ethynylpyrene)benzene (BP molecule) in chloroform-D**

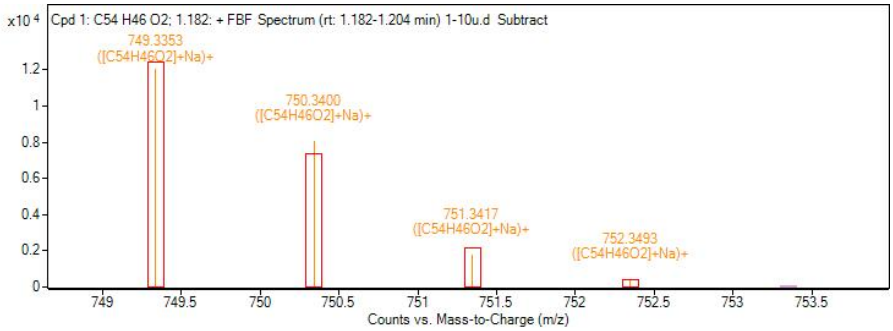


**Supplementary Fig. 5 HR-MS of 1,4-bis(hexyloxy)-2,5-bis(ethynylpyrene)benzene (BP molecule)**

## Supplementary Note 2. Device fabrication and characterization

The device fabrication process is summarized in Supplementary Figure 6. A 4-inch silicon wafer (with a 500 nm oxide layer) was utilized for photolithography and electron beam evaporation to fabricate a 30 nm thick gold back-gate array with an adhesion layer of 10 nm titanium. A 10 nm insulating layer of $HfO_2$ was deposited using an atomic layer deposition system. Subsequently, a second array of 60 nm thick gold source and drain electrodes with an adhesion layer of 10 nm titanium was fabricated by wafer-level alignment of photolithography and electron beam evaporation. The silicon wafer was sliced into chip units for further fabrication of graphene electrodes.

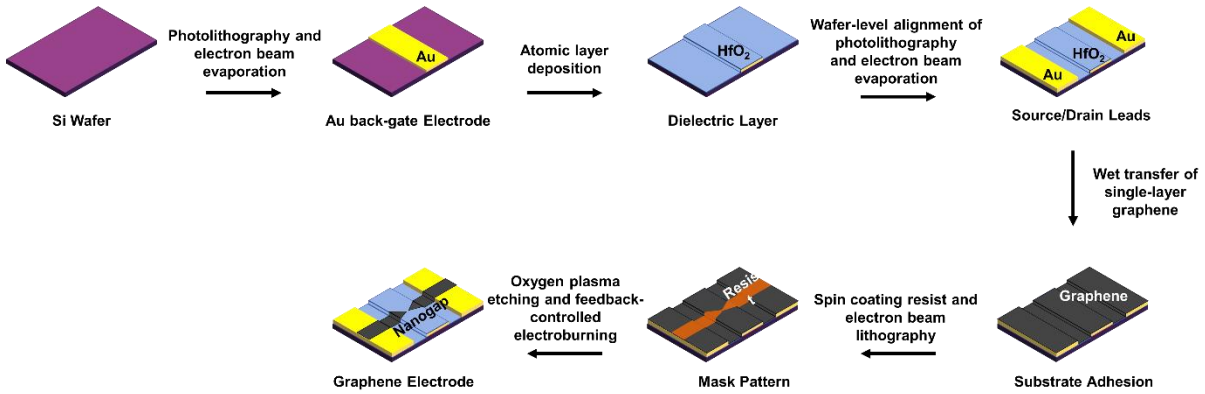


**Supplementary Fig. 6 Schematic diagram of the preparation process for the graphene electrode and gold back gate before assembling molecules**

The monolayer graphene (MLG) was grown using chemical vapor deposition (CVD, Equipment Corporation ET3000EXT) on a copper foil. Subsequently, the copper foil was cut into a suitable size after spin-coating with PMMA. The copper foil was etched with ammonium persulfate solution (7.2 g $(NH_4)_2S_2O_8$ in 80 mL $H_2O$) for 24 hours and then washed with deionized water three times to remove residual etching solution. The pre-processed silicon unit was used to pick up the PMMA/MLG sheet, which was then immersed in acetone to remove the PMMA three times. By using mixed hydrogen-argon gas and annealing at 210 ℃ for 3 hours, the PMMA residue was removed and some graphene defects were reduced. The negative resist ma-N 2403 (Micro Resist Technology) was used for electron beam lithography to write bowtie patterns on the MLG on the silicon unit after development by the ma-D 525 (Micro Resist Technology). The areas not covered by the resist were etched using $O_2$-plasma to produce the MLG bowtie pattern. Subsequently, the sample was immersed in mr-Rem 700 (Micro Resist Technology) for 30 s and washed with acetone and ethanol to remove the residual resist. Utilizing the feedback-controlled electroburning, the graphene bowtie was further processed to produce a 1-2 nm gap in the narrowest constriction area, resulting in a graphene nanoelectrodes pair with resistance in the range of hundreds of megaohms. The processing method follows the procedures outlined in previously published work [4]. Further current-voltage characterization before and after depositing molecules are performed in room temperature. More detailed characterizations of the devices are displayed in Supplementary Figure 7. The ultraviolet-visible absorption and luminescence spectrum summarized in Supplementary Figure 10. The yield of single-molecule junctions is 4% (6/150) according to room-temperature *I-V* characteristics. Due to the different coefficients of thermal expansion of graphene and $HfO_2$, the contact configuration between graphene and $HfO_2$ changes during the cooling down, leaving only two molecules still surviving after the temperature drops to 30 K[5]. In such a single-molecule

transistor geometry, the gate coupling efficiency α is approximately 0.3 based on the slopes of the Coulomb diamond boundaries.

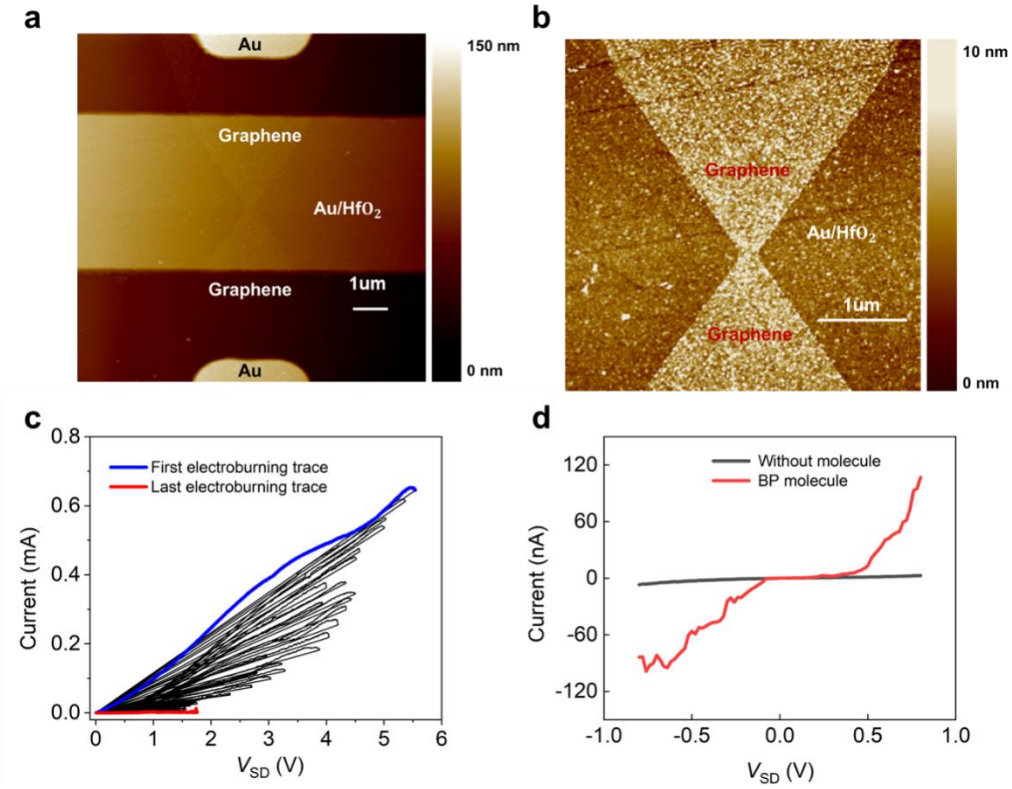


**Supplementary Fig. 7 Characterizations of device fabrication**. **a**, Characterization of patterned graphene at core area using Atomic force microscope (AFM) images of 10 μm × 10 μm region, with graphene serving as the source-drain electrodes and gold contacting both sides, with the underlying gold serving as the gate electrode. **b**, Characterization of AFM image of the 4 μm × 4 μm region at the center of graphene constriction, with RMS-roughness: 1.62 nm (graphene) and 0.87 nm ($HfO_2$). **c**, Feedback-controlled electroburning traces of graphene bowtie. **d**, Room temperature *I-V* traces before (black lines) and after (red lines) depositing molecules.

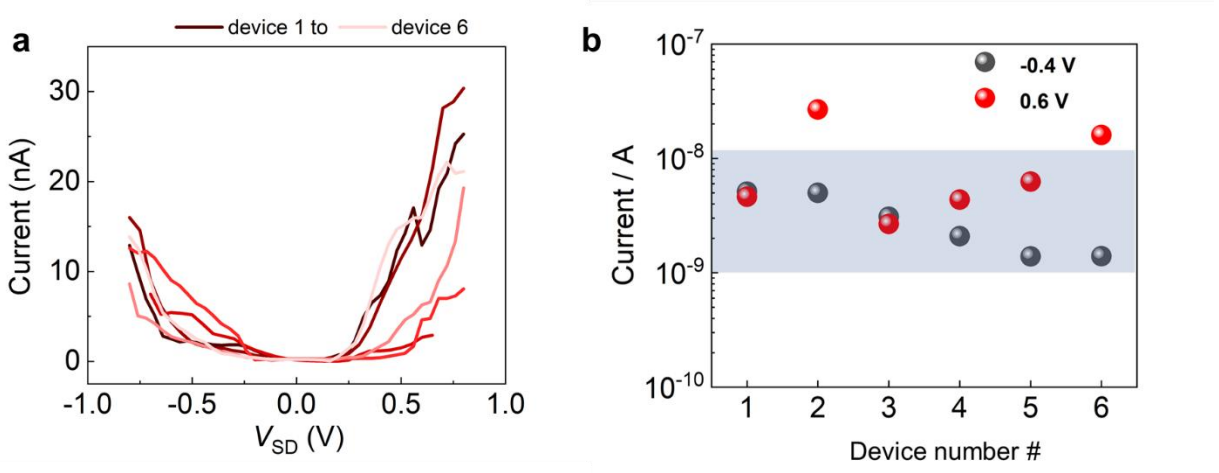


**Supplementary Fig. 8 Characterizations of *I-V* traces (a) and Current magnitude difference (b) among six devices at 30 K on a continuous $V_G$ = 0 V.**

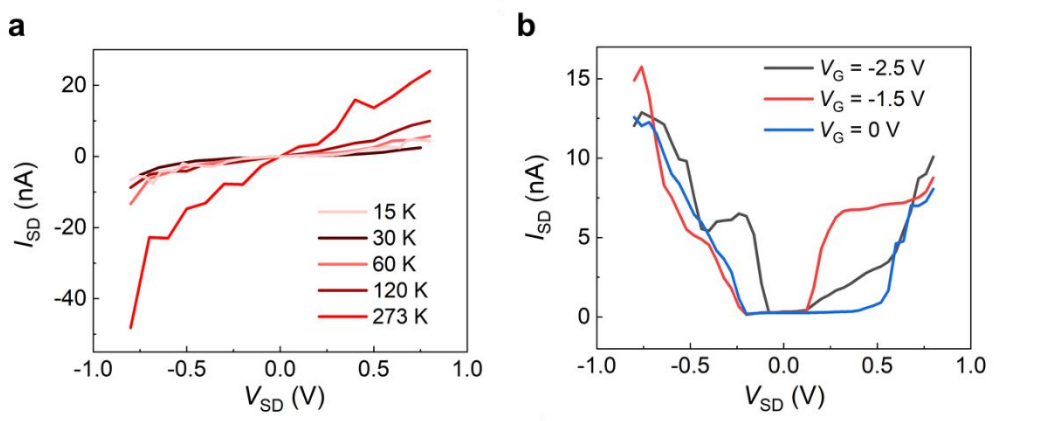


**Supplementary Fig. 9 Temperature and gating voltage dependent current-voltage curves of device 1. a,** *I-V* curves at different temperatures **(**273 K, 120 K, 60 K, 30 K, 15 K**). b,** *I-V* curves at different gating voltage $V_G$ (0 V, -1.5 V, -2.5 V) at 30 K.

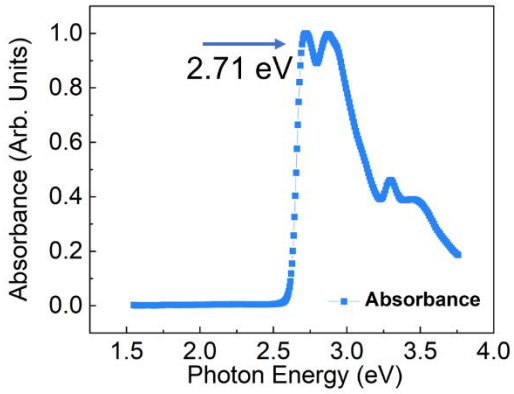


**Supplementary Fig. 10 Absorption spectra of BP molecule.**

**Supplementary Note 3. Details of single-pulse measurement**

Varying the voltage pulse width could be used in principle to characterize the charged excited states dynamics, which has been demonstrated in probing the triplet quenching in individual pentacene[6]. Therefore, we performed the voltage pulse-width dependence measurements using a $V_{pulse}$ = −0.8 V, as shown in Supplementary Figure 12. Since current grows with the increase of pulse width (Supplementary Figure 12, a-b), we normalized the relationship between $I_{pulse}$ and $\tau_{pulse}$ by extracting the amount of current change caused by unit pulse width, $I_{pulse}/\tau_{pulse} = (I_{pulse} - I_{\tau=0\ ns})/\tau_{pulse}$. The signal at $\tau_{pulse}$ = 0 ns is subtracted in order to minimize the impact of rising and falling edges on the accuracy of normalization. The normalized $I_{pulse}$ at $V_G$ = 0 V corresponding to the N state is insensitive to the pulse width. In contrast, a low-to-high dynamical curve of normalized $I_{pulse}$ appears at $V_G$ = − 2.5 V and the single-exponential fitting reflects a lifetime of ~86 ns (Supplementary Figure 12c).

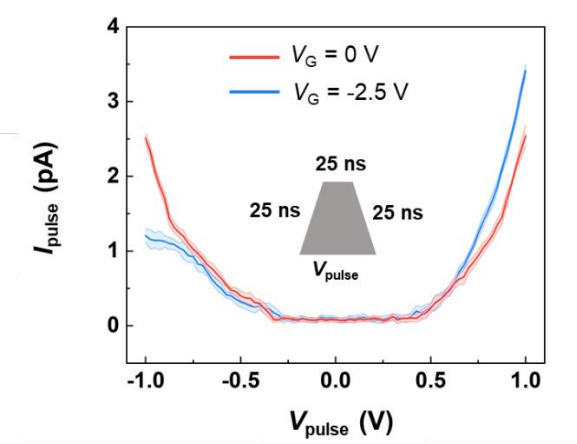


**Supplementary Fig. 11** Pulse current-voltage characterizations at N−1 (blue line, $V_G$= −2.5 V with the error range indicated by the blue shaded area) and N (red line, $V_G$= 0 V with the error range indicated by the red shaded area ) states of BP molecule.

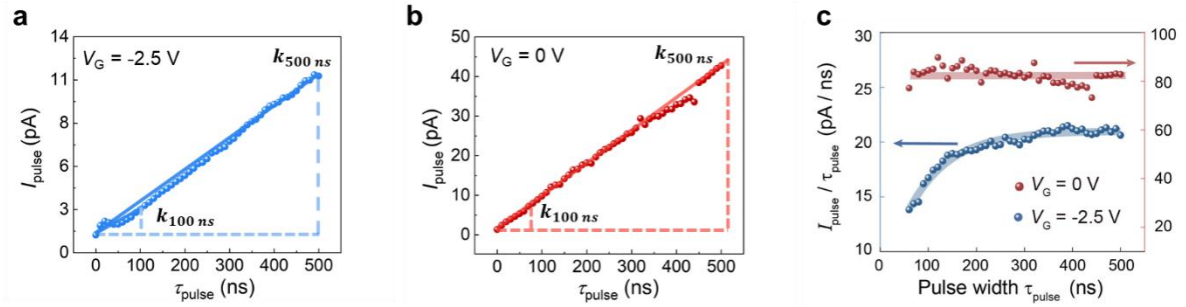


**Supplementary Fig. 12 Single-pulse measurement of the charged single molecule by pulse-width dependence experiment. a**,**b**, Measured pulse current $I_{pulse}$ as a function of pulse width $\tau_{pulse}$ with fixed −0.8 V amplitude at $V_G$= −2.5 V (**a**) and 0 V (**b**). **c**.The normalized pulse current by variable pulse width voltage at $V_G$ = −2.5 V (blue line) and 0 V (red line). The red and blue lines are guides for the eye. The normalization method was to extract the slope of the signal difference under different pulse widths compared to that at $\tau_{pulse}$ = 0 ns.

**Supplementary Note 4. Pump-probe measurement of different devices of BP molecule**

To verify the reproducibility of the observed dynamic phenomena, we fabricated another BP single-molecule transistor device (**Device 2**) and performed steady-state differential conductance measurements within a voltage window of ±0.8 V. The results are shown in Supplementary Figure 14a. We noted that the gate voltage at which the transition between the $N$ and $N$−1 charge states occurs at the gate voltage of $V_{cross}$ = −2.5 V, which is very close to that of **Device 1**, with only minor differences. These differences may arise from slight variations in the molecular conformation during the assembly process. Under $V_G$=−2.5 V, the dynamic behavior of **Device 2** shown in Supplementary Figure 14b was essentially consistent with the phenomena previously observed (**Fig. 2e**). We further performed the gate control of lifetime in another BP device (**Device 3**) shown in Supplementary Figure 15. We observe the relaxation dynamics appears when the gate voltage is approaching the resonance transport and saturate when the charge state is stabilized in Coulomb blockade regime. The non-step like gate-dependence near the state cross point demonstrates the electrostatic potential change can effectively control the lifetime of excited states in single molecule.

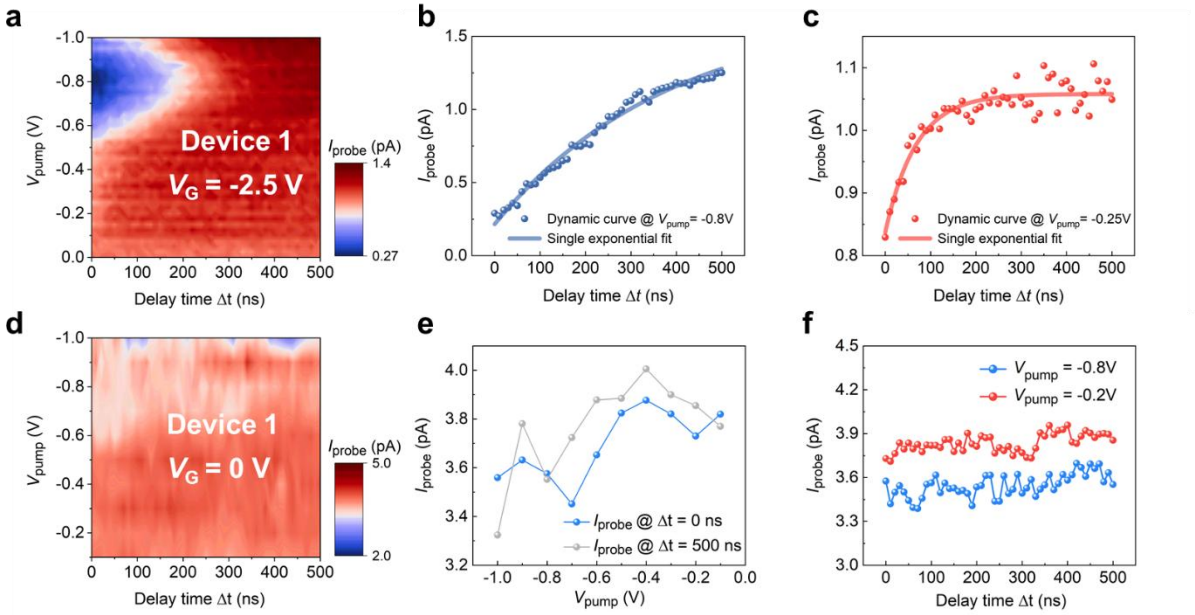


**Supplementary Fig. 13 All-electronic pump-probe measurements of the BP molecule in device 1. a**, Corresponding dependence of the probe current $I_{probe}$ on the delay time as a function of trigger voltage $V_{pump.}$ at a continues $V_G$ = −2.5 V. **b**, Single pump–probe spectra under a pump voltage of −0.8 V and its single-exponential fitting curve. **c**, Single pump–probe spectra under a pump voltage of −0.25 V and its single-exponential fitting curve. **d**, Corresponding dependence of the probe current $I_{probe}$ on the delay time as a function of trigger voltage $V_{pump.}$ at a continues $V_G$ = 0 V. **e**, Corresponding dependence of the probe current $I_{probe}$ at $\Delta t$ = 0 and 500 ns as a function of trigger voltage $V_{pump}$ of a neutral **BP** molecule. **f**, Corresponding dependence of the probe current $I_{probe}$ as a function of the delay time at $V_{pump}$ = −0.2 and −0.8 V.

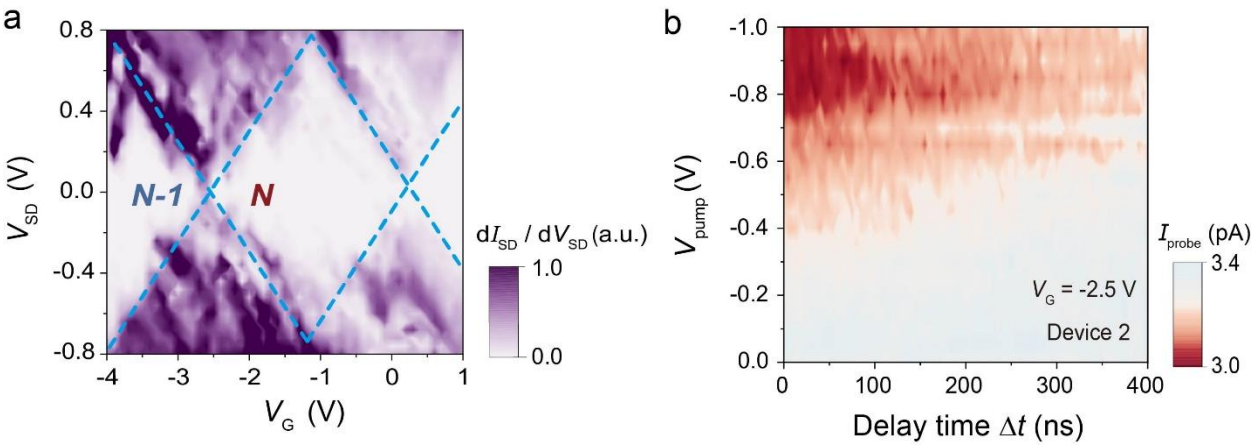


**Supplementary Fig. 14 All-electronic pump-probe measurements of the BP molecule in device 2. a.** Charge stability diagram of device 2 showing the differential conductance ($dI_{SD}/dV_{SD}$) as a function of bias voltage ($V_{SD}$) and gate voltage ($V_G$) at 30 K. **b**, Corresponding dependence of the probe current $I_{probe}$ on the delay time as a function of trigger voltage $V_{pump.}$ at a continues $V_G$ = −2.5 V. Similar feature with **Device 1** could be observed in **b,** where an obvious low conducted state was found around $V_{pump}$ = −0.8 V**.**

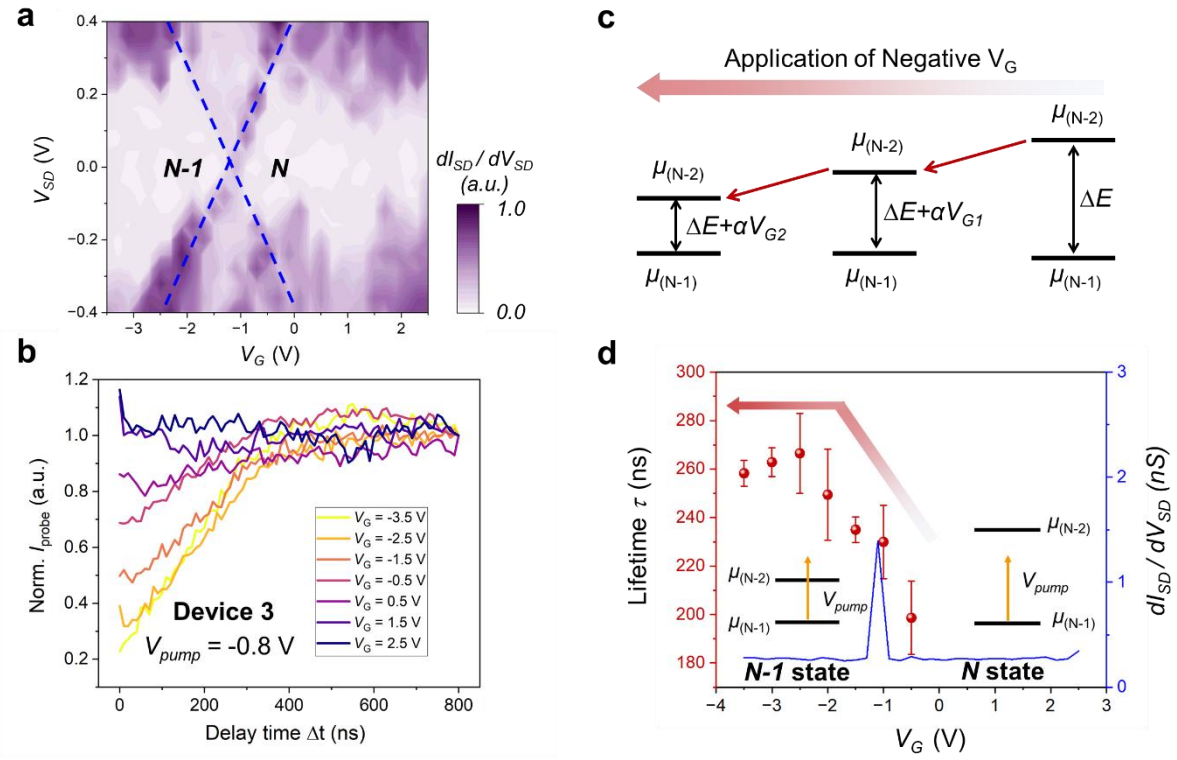


**Supplementary Fig. 15 All-electronic pump-probe measurements of the BP molecule in device 3. a.** Charge stability diagram of device 3 showing the differential conductance ($dI_{SD}/dV_{SD}$) as a function of bias voltage ($V_{SD}$) and gate voltage ($V_G$) at 30 K. **b**, Corresponding dependence of the probe current $I_{probe}$ on the delay time as a function of gate voltage $V_{gate.}$ at a fixed pump voltage

$V_{pump}$ = −0.8 V. **c**, Many-body energy diagram illustrating gate-induced modulation, in which the energy gap between the $N-1$ and $N-2$ states decrease as a negative gate voltage $V_G$ applied. **d**, Differential conductance ($dI_{SD}/dV_{SD}$) at $V_{SD}$ = 0 V (blue line) and the lifetime of electrically excited states (red dots) with error bar as a function of continuous gate voltage $V_G$. The lifetime is extracted from the dynamics curves in Supplementary Figure 15b. The error bars represent the uncertainty associated with the single-exponential decay fitting. The peak around $V_G \approx -1$ V in the differential conductance indicates the transition from the N state to the $N-1$ state. Under the condition of a fixed $V_{pump}$, sweeping the gate voltage $V_G$ directly tunes the energy difference between the two different charge states. Correspondingly, the transient dynamics become pronounced at $V_G < -1$ V, since the population of the $N-1$ state is negligible for $V_G > -1$V. The lifetime initially exhibits an upward trend (between −0.5 V to −2 V) because of the energy broadening of the involved state, which signifies a growing population of the excited state as the voltage increases. However, once the excitation energy provided by exceeds the energy broadening of the excited state, the population and therefore the lifetime reaches a plateau and remains almost entirely unchanged (between −2.5 V to −4 V).

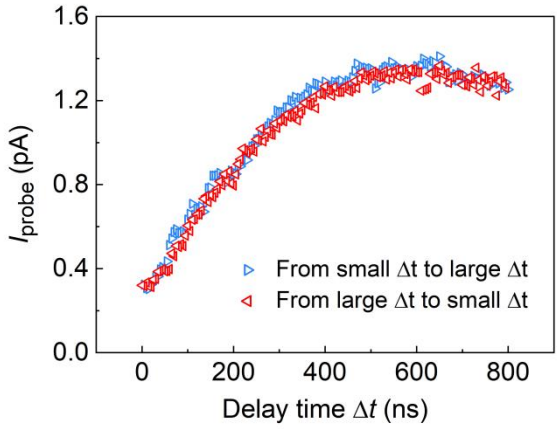


**Supplementary Fig. 16 Forward and reverse scan of pump–probe spectra**. The blue triangle represents the signal response of the probe current increasing from 0 ns to 800 ns with 10 ns intervals, where red triangle represents the opposite.

**Supplementary Note 5. Details of Calculation Methods**

As shown in Supplementary Figure 17a, the alkane branched chains of **BP** molecule was simplified due to its small impact on energy levels but not conducive to convergence during optimization. We considered various initial structures of the **BP** molecule, the configuration with the symmetry of $C_{2h}$ has the lowest energy after relaxation (Supplementary Figure 17b). Then, the energy levels and electron distribution of **BP** molecular frontier orbitals are also calculated and shown in Supplementary Figure 17c. The calculated energy difference of HOMO and LUMO is 2.73 eV, which is consistent with the bandgap of 2.71 eV observed in the Ultraviolet-Visible spectrum (Supplementary Figure 10).

For neutral molecule, the excitation energies of the lowest three excited states are calculated by TDDFT method adopted in Gaussian 16, with $T_1 - S_0 = 1.65$ eV, $T_2 - S_0 = 1.89$ eV, $S_1 - S_0 = 2.50$ eV. We also calculate the energy of $T_1$ state by DFT method adopted in Gaussian 16, with $T_1 - S_0 = 1.71$ eV, which is consistent with the TDDFT results. The excitation energies of the lowest three excited state for $\mathbf{BP^+}$ are calculated to be $D_1^+ - D_0^+ = 0.82$ eV, $D_2^+ - D_0^+ = 1.11$ eV, $D_3^+ - D_0^+ = 1.51$ eV. While the excitation energies of the lowest two excited state for $\mathbf{BP^{2+}}$ are $T_1^{2+} - S_0^{2+} = 0.11$ eV, $S_1^{2+} - S_0^{2+} = 0.92$ eV.

**Supplementary Table 1 Calculated energy variations relative to $\mathbf{D_0^+}$ due to molecule geometries.** The **BP** molecule geometries are optimized under different external electric fields (E = 0.8 V and 0 V).

| $D_0^+$ | $S_0$ | $D_1^+$ | $D_2^+$ | $S_0^{2+}$ | $T_1^{2+}$ |
|---|---|---|---|---|---|
| 0 eV | -0.07 eV | +0.02 eV | +0.02 eV | 0 eV | +0.01 eV |

**Supplementary Table 2 Calculated dipole moments of N, N − 1 and N − 2 states.** The **BP** molecule geometries are optimized under different external electric fields (E = 0.8 V and 0 V).

| E | N state ($S_0$) | N–1 state ($D_0^+$) | N–2 state ($S_0^{2+}$) | N–2 state ($T_1^{2+}$) |
|---|---|---|---|---|
| 0.8 V | -5.12 Debye | -14.37 Debye | -14.20 Debye | -11.64 Debye |
| 0 V | 0 Debye | 0 Debye | 0 Debye | 0 Debye |

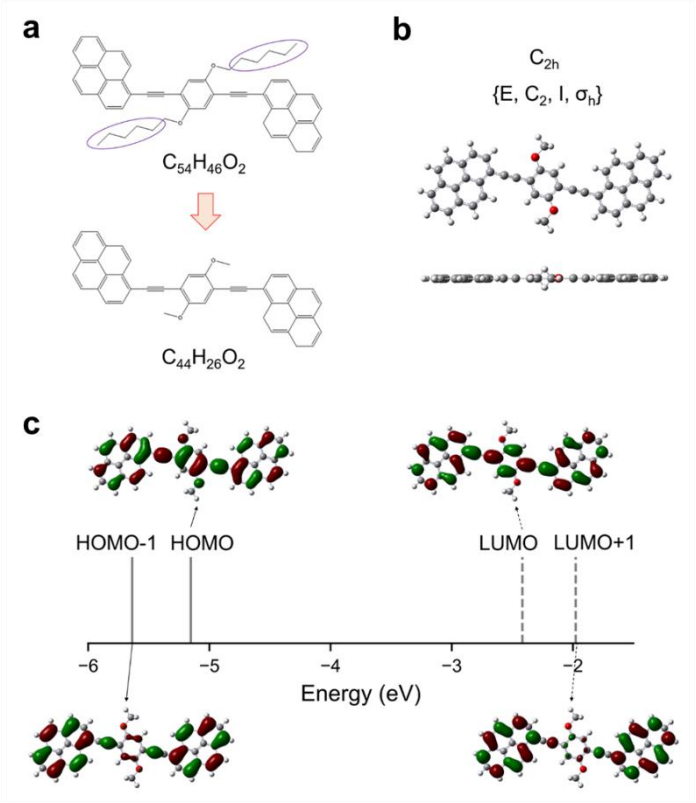


**Supplementary Fig. 17 Calculated molecular structure and frontier orbitals of BP molecule**. **a**, Schematic diagram of structural simplification. **b**, The top view, side view and symmetry of **BP** molecule. **c**, Energy level and molecular frontier orbitals of **BP** molecular frontier orbitals.

According to the calculation results, we plot the energy alignment between electrode and molecule is shown at Supplementary Figure 18 in a single-particle picture. The resonant peaks occur in **Fig.4** corresponds to the transition from $T_1^{2+}$ and $S_0^{2+}$ to $D_n^{+}$ in a many-body picture.

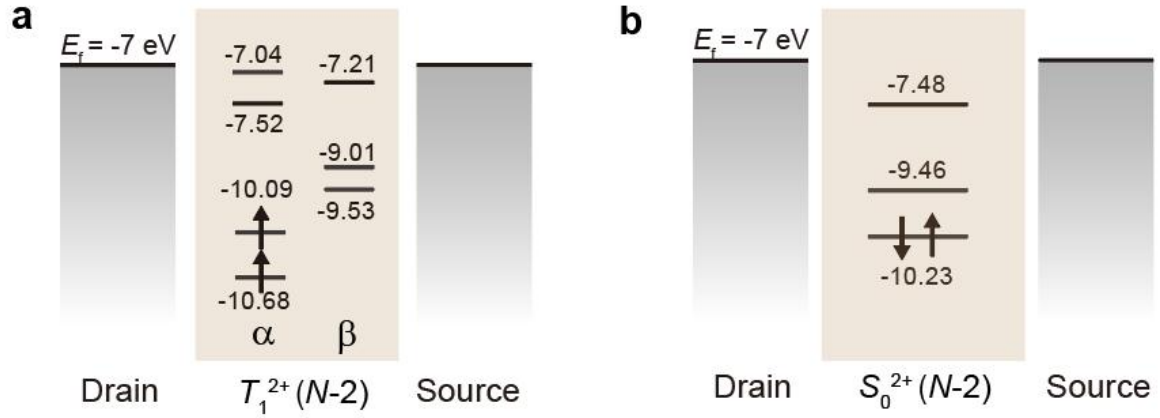


**Supplementary Fig. 18 Single-particle illustration of energy alignment between (a) $T_1^{2+}$ and (b) $S_0^{2+}$ with electrodes derived from TDDFT calculations**

To exclude the contribution of structural relaxation-induced changes in the energy level structure, we optimized the molecular junction configurations for different charged states. For isolated molecules, the structures showed negligible variation across charged states, necessitating investigation of electrode-coupled configurations. We employed hydrogen-saturated graphene fragments as electrodes and optimized the molecular junction using the B3LYP-D3(BJ) functional with the 6-31G(d) basis set. The initial electrode separation was set to ~10.9 Å (C···C distance, matching the spacing between two pyrene groups in the molecule). During optimization, we fixed the electrodes while allowing the molecule to relax without constraints, simultaneously applying a 1 V/nm electric field along the electrode axis.

As shown in Supplementary Figure 19, electrostatic interactions between oxygen atoms and hydrogen atoms on the graphene electrodes induced rotation of the central benzene ring in the molecule, with distinct dihedral angles observed for different charged states. Additionally, charged states exhibited varying stacking offsets relative to graphene, particularly pronounced for $T_1^{2+}$. Using these optimized structures, we calculated single-electron energy level changes before and after structural relaxation within the same electronic state. The structural modifications were found to induce negligible energy level and state energy shifts (Supplementary Figure 20 and Supplementary Table 3, mostly <0.1 eV), thereby confirming that configurational relaxation of the molecular junction contributes negligibly to the electronic energy levels.

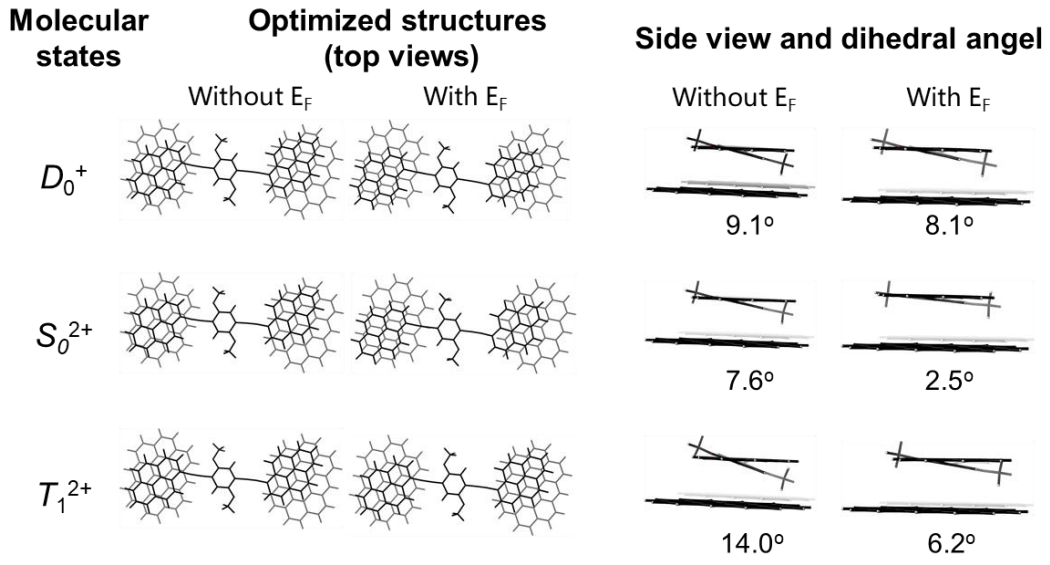


**Supplementary Fig. 19 Optimized structures of molecular junctions for different charged states.**

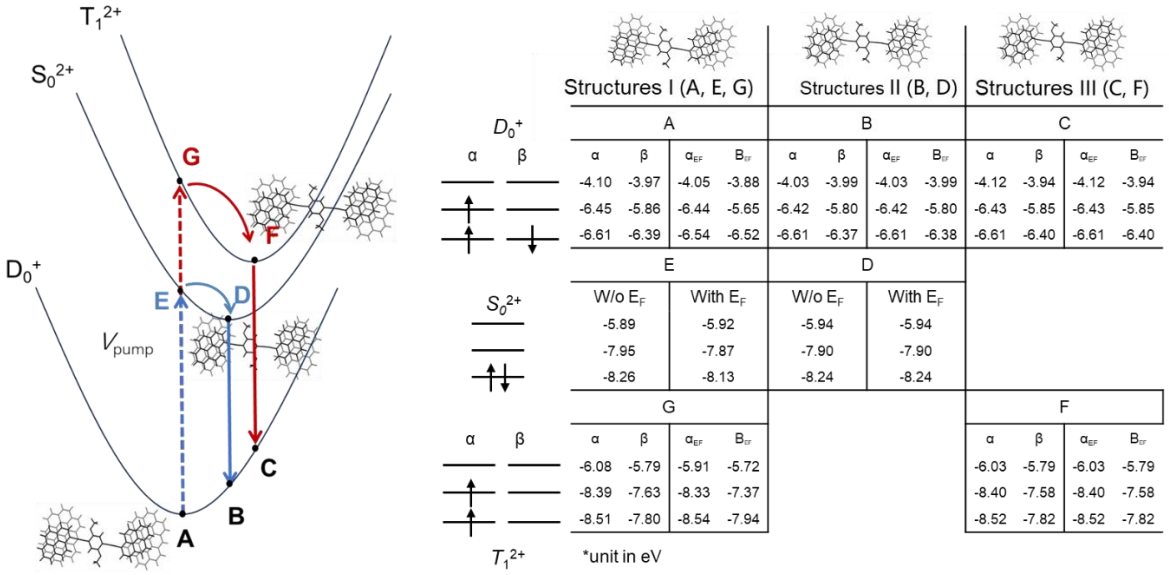


**Supplementary Fig. 20 Energy level of single molecule in molecular junctions for different charged states and structure.**

**Supplementary Table 3 Calculated energy variations due to molecule geometries.**

| $\Delta E_E - \Delta E_D$ | $\Delta E_G - \Delta E_F$ | $\Delta E_C - \Delta E_A$ | $\Delta E_B - \Delta E_A$ |
|---|---|---|---|
| 0.0174 eV | 0.0463 eV | 0.1204 eV | 0.0600 eV |

## Supplementary Note 6. Data processing of Transient *I-V*

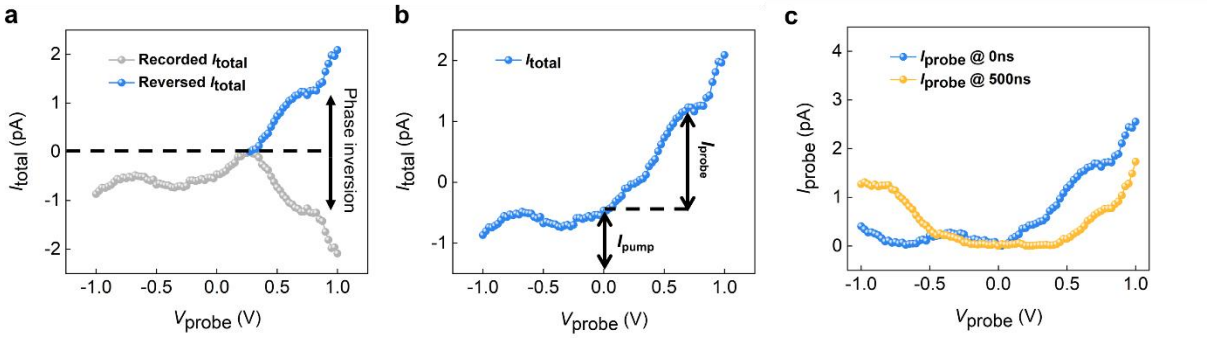


**Supplementary Fig. 21 Transient $I_{pulse}$-$V_{pulse}$ pump-probe measurements of the charged molecule**. **a**, Total current $I_{total}$ recorded in a lock-in amplifier before (gray) and after (blue) considering phase inversion. **b**, Total current after considering phase inversion and the method for extracting probe current. **c**, Transient pulsed *I-V* characterization at 0 ns (blue) and 500 ns (yellow).

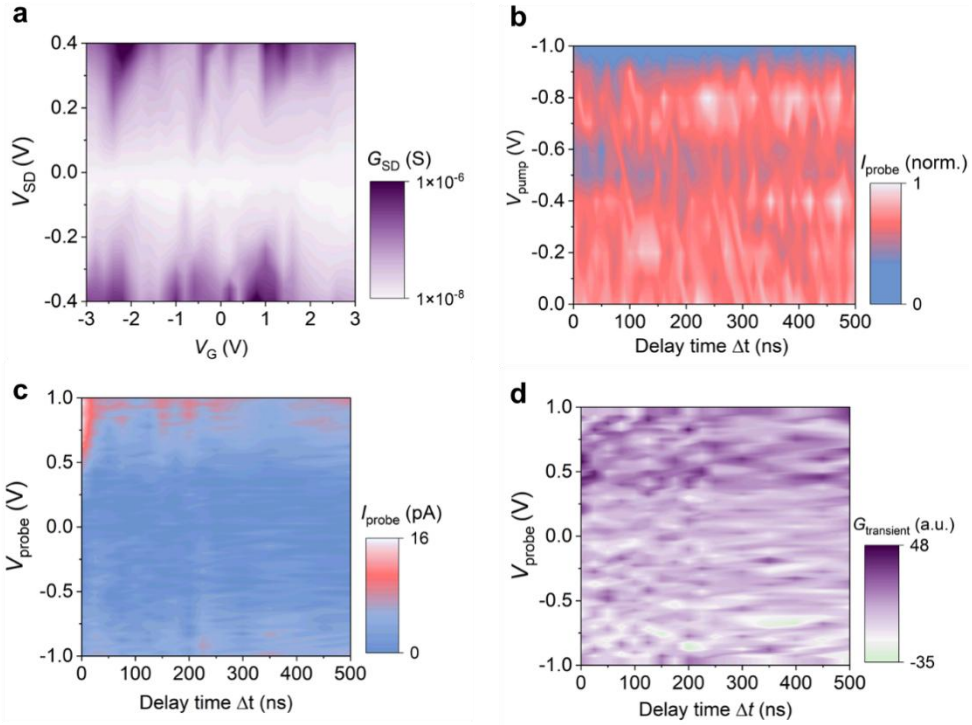


**Supplementary Fig. 22 Electrical characterizations and all-electronic pump-probe measurements on a graphene tunnel junction. a**, Charge stability diagram showing the differential conductance $G_{SD}$ ($dI_{SD}/dV_{SD}$) as a function of bias voltage ($V_{SD}$) and gate voltage ($V_G$) at 30 K. **b**, Corresponding dependence of the probe current $I_{probe}$ on the delay time as a function of trigger voltage $V_{pump}$ at a continuous $V_G = 0$ V. **c**, Corresponding dependence of the probe current $I_{probe}$ on the delay time as a function of probe voltage $V_{probe}$ at a continuous $V_G = 0$ V. **d**, Transient differential conductance spectroscopy $G_{transient}$ ($dI_{probe}/dV_{probe}$) of graphene tunneling junction.

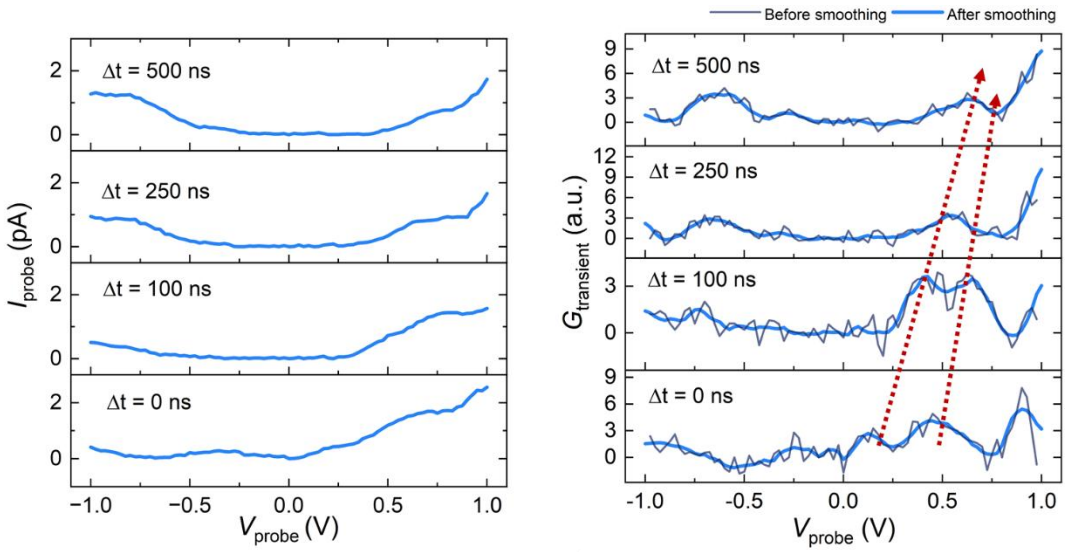


**Supplementary Fig. 23** The differential conductance (right panel) derived from $I_{probe}$-$V_{probe}$ curves (left panel) before (black) and after (blue) smoothing The red dashed lines indicate the movement of resonance peak over time.

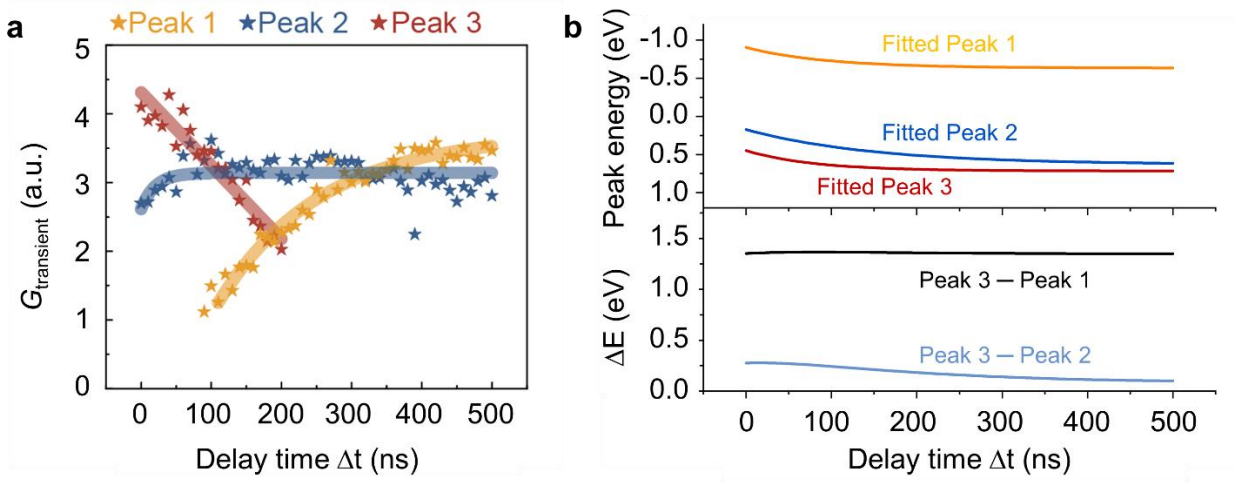


**Supplementary Fig. 24** The time evolution of peak intensity (a), energy (top panel of b) and energy space (bottom panel of b) among Peak 1, Peak 2 and Peak 3 shown in Fig. 4b.

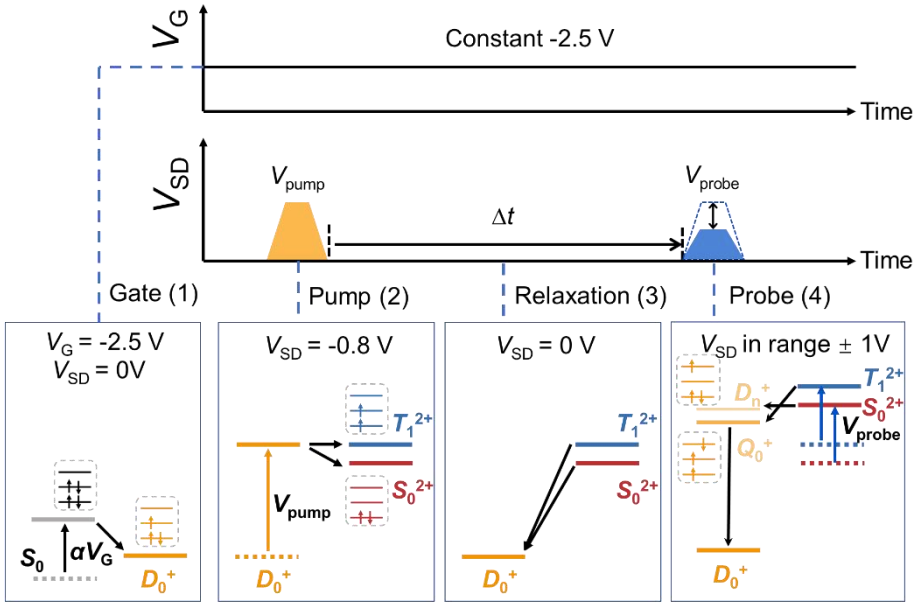


**Supplementary Fig. 25 The role of the four measurement stages: Gate, Pump, Relaxation (Delay), and Probe.** The continuous gate voltage sets the system near the charge degeneracy point, enabling the transition from *N* state to *N-1* state. The Pump pulse serves to trigger the excitation and varying the pump voltage allows us to determine the energy threshold required to access the excited state. During relaxation stage (In delay time stage, bias is equal to 0 V), the excited state undergoes spontaneous relaxation back to the ground state. The Probe pulse is employed to detect the relaxation dynamics of the transient states and varying the probe voltage allows us to map the *I-V* characteristics of the transient species (e.g., at $\Delta t$ = 0 ns, the population of the charged excited state $S_0^{2+}$/ $T_1^{2+}$ is dominant).

**References:**


1. Wu W., Sun J., Ji S., Wu W., Zhao J., Guo H. Tuning the emissive triplet excited states of platinum(ii) schiff base complexes with pyrene, and application for luminescent oxygen sensing and triplet–triplet-annihilation based upconversions. *Dalton Trans.* **40**, 11550 (2011).
2. Gopi A., Sajitha M., Haridas R., Varghese L., Yoosaf K. Cooperative and fret-assisted brightness enhancement in oligo(phenylene ethynylene): Quantum dot organic–inorganic nanohybrids. *Chem. Asian J.* **13**, 1492 (2018).
3. Constantinescu C., Diallo A. K., D'Aleo A., Fages F., Rotaru P., Videlot-Ackermann C., *et al.* Thermal behaviour and thin film properties of a bis-pyrene compound for organic thin film transistor applications. *Synth. Met.* **209**, 29 (2015).
4. Thomas J. O., Limburg B., Sowa J. K., Willick K., Baugh J., Briggs G. A. D., *et al.* Understanding resonant charge transport through weakly coupled single-molecule junctions. *Nat. Commun.* **10**, 4628 (2019).
5. Limburg B., Thomas J. O., Holloway G., Sadeghi H., Sangtarash S., Hou I. C.-Y., *et al.* Anchor groups for graphene-porphyrin single-molecule transistors. *Adv. Funct. Mater.* **28**, 1803629 (2018).
6. Peng J., Sokolov S., Hernangómez-Pérez D., Evers F., Gross L., Lupton J. M., *et al.* Atomically resolved single-molecule triplet quenching. *Science* **373**, 452 (2021).